Advanced Engineering Science
http://publish.mersin.edu.tr/index.php/ades
e-ISSN 2791-8580

Influence of antimony doping on structural, morphological and optical properties of CuO powders

Saadet Yıldırımcan *[1]

[1]*Mersin University, Institute of Science, Department of Nanotechnology and Advanced Materials, Türkiye, syildirimcan@mersin.edu.tr*
[2]*Mersin University, Vocational School of Technical Sciences, Department of Medical Services and Techniques, Program of Opticianry, Türkiye*

Cite this study: Yıldırımcan, S. (2024). Influence of antimony doping on structural, morphological and optical properties of CuO powders. Advanced Engineering Science, 4, 120-129

Keywords
CuO
Antimony
Doping
Powder
Chemical bath deposition

Research Article
Received: 20.07.2024
Revised: 25.08.2024
Accepted: 01.09.2024
Published: 04.09.2024

Abstract

In this study, pure and antimony (Sb) doped CuO nano and micro powders were produced by chemical bath deposition (CBD) technique. Their structural, morphological, elemental and optical properties were examined using XRD, SEM, EDX and UV-Vis techniques. According to crystallographic structure analysis, the pure and Sb doped CuO powders were obtained in monoclinic phase. The crystallite size of the powders decreased with the Sb concentration. The FE-SEM images clearly show that flower-like structures in both pure and Sb doped CuO powders were grown. Moreover, the EDX spectra show that the peak intensity of Sb increases upon increasing doping concentration of Sb. The band gap energy value of the powders increased from 1.58 eV to 1.95 eV with increased Sb concentration in CuO. In addition, the key optical parameters such as refractive index, extinction coefficient, and both real and imaginary parts of the dielectric constant were calculated.

1. Introduction

Recently, researchers have intensified studies in the field of energy with the advancement of nanotechnology. In particular, studies on transition metal oxides, aimed to increasing solar cell efficiency, attract much attention. Among these metal oxides, copper oxide is widely used for applications such as photocatalysis [1], gas sensor [2], water splitting [3] and solar cells [4] due to its excellent properties such as chemical and thermal stability, low thermal emittance, optical properties, high photoactivity, low toxicity, and low-cost production [1]. Copper oxides are important monoclinic p-type transition metal oxide semiconductors, having a narrow band gap of 1.21 - 2.00 eV [5, 6].

The crystal structure, optical and electrical properties of CuO can be improved by doping with elements such as Mn, Co, Ni, Zn, Sb and Fe [7-10]. Antimony is a favored dopant element in CuO nanoparticles for electronic and optical applications, thanks to its outstanding properties and ability to modify the material's characteristics [11, 12]. Introducing Sb atoms into the CuO lattice tailors its physical characteristics, enabling advanced applications in electronics, photonics, catalysis, and energy storage [11, 13-16].

There is limited knowledge in literature on the characteristic properties of Sb-doped CuO [9, 11, 13]. Baturay et al. fabricated Sb-doped CuO thin film with 0, 1, 2 and 3 wt% of Sb doping concentrations by spin coating technique. They investigated morphological, structural, and optical properties of the samples and reported that there is a radical increase in the energy band gap of the obtained films from 1.70 to 2.37 eV [13]. Pandey et al. [15] were synthesized CuO-ZnO nanocomposites with different Sb concentration using sol-gel method and investigated electrical properties along with optical properties and magneto-dielectric properties for technological applications. They reported that the band gap energy was 2.48 eV for pure CuO-ZnO, 2.39 eV for 2.5% Sb doped and 2.32 eV for 5% Sb doped CuO-ZnO [15]. In another study, Baek et al. produced a double-layer photocathode thin film containing Sb-doped Cu_2O and undoped Cu_2O. The Cu_2O single layer had a current density of 0.1 mA/cm^2

(applied voltage: +3 V), while Cu_2O:Sb/Cu_2O exhibited 1.37 mA/cm^2 [17]. Novel studies on Sb-doped CuO will reveal new possibilities for technological applications.

There is various method for the synthesis of CuO and its derivatives such as sol–gel [18], thermal oxidation [19], electro-deposition [20], chemical bath deposition [21], spray-pyrolysis [22], co-precipitation [23]. In this study, the CBD method was used because of its simplicity, controllability, and eco-friendly. The pure and Sb doped CuO powders were synthesized using the CBD method. The structural, morphological, elemental and optical properties were studied using X-ray powder diffractometer (XRD, Rigaku, Smartlab), FE-SEM (QUANTA 400F Field Emission SEM), energy dispersive X-ray EDX (QUANTA 400F) spectroscopic and UV-Vis spectrophotometric techniques. The aim of this study is to improve the characteristic properties of CuO for solar cells by doping with different Sb concentrations.

2. Material and method

2.1. Materials

Copper(II) Acetate Monohydrate ($Cu(CO_2CH_3)2H_2O$, Merck, 98%), Antimony(III) Chloride ($SbCl_3$, Sigma-Aldrich, 99%) and Ammonia solution (NH_4OH, Merck, 25%) were used to produce pure and Sb doped CuO powders.

2.2. Synthesis of the pure CuO and Sb doped CuO powders

0.1 M Copper(II) acetate monohydrate ($Cu(CO_2CH_3)2H_2O$) was dissolved in 100 ml of ultra-distilled water to prepare solution. The pH was adjusted to 11 by adding NH_4OH to the prepared solution. The solution was stirred at 90°C for 20 min. Finally, the resulting powders were dried at 90°C for 1 hour and then annealed at 450°C for 2 hours. In this study, the preferred annealing temperature was 450°C [24]. The same procedure was used to produce Sb-doped CuO powders at 1 at.% and 3 at.% concentrations. Within the text, the samples are labeled as S1, S2, and S3 for pure CuO, 1 at.% Sb, and 3 at.% Sb doped CuO, respectively.

3. Results and discussion

3.1. Structural properties

The crystallographic structure analyzes of all samples were performed by the XRD technique, as shown in Figure 1(a) and (b). Based on XRD patterns, the pure and Sb-doped CuO powders exhibit monoclinic phase with C2/c space group (JCPDS: 048–1548) [25]. The peaks at 32.5, 35.5, 38.7, 48.7, 53.5, 58.3, 61.5, 66.2, 68.1, 72.4, and 75° correspond to the (110), (002), (111), (20-2), (020), (202), (11-3), (31-1), (220), (311), and (004) planes of the monoclinic phase. Similar peaks have been observed in previous studies [25-28]. In addition, the strongest XRD peaks occurred at (002) and (111) plane for all powders. It was noticed that the XRD peaks of the pure CuO shifted towards larger angle with Sb doping and the peak intensity of Sb doped CuO powders decreased gradually with increasing Sb concentration (Figure 1(b)). Moreover, no phase change was observed in any of the nano/micro powders, and no second phase was occurred. In other words, Sb doping did not induce any phase changes in the crystal structure of CuO (Figure 1(a)).

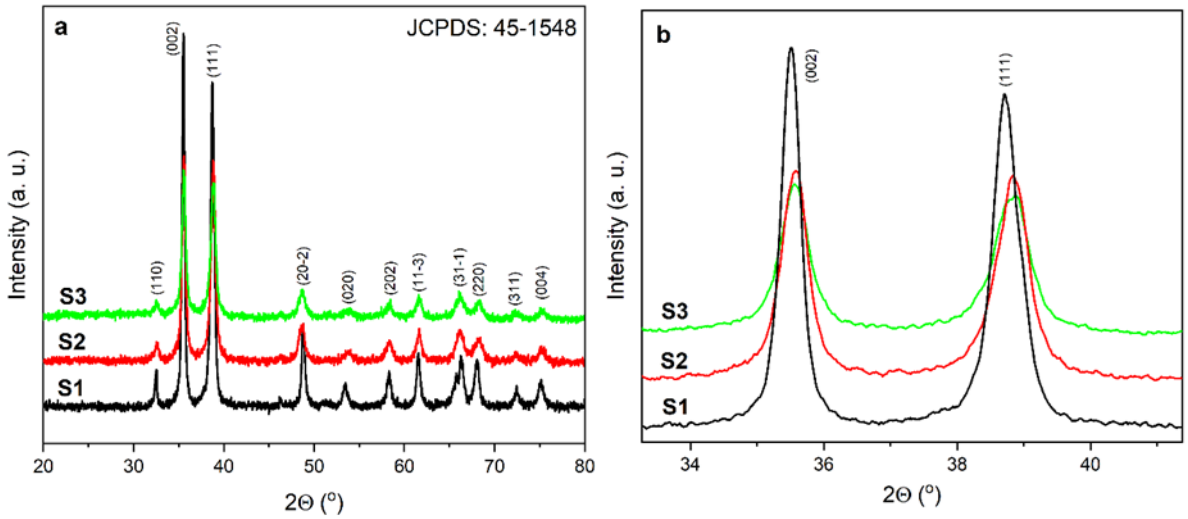

Figure 1. (a) The XRD patterns of the pure and Sb doped CuO powders, (b) expanded view of the strongest peaks.

The crystallite size, strain, dislocation density, and lattice parameters of the pure and Sb doped CuO powders were calculated and provided in Table 1. Scherrer formula (Equation (1)) based on the strongest peak (002) was used to calculate crystallite size [29]:

$$D_{hkl} = \frac{k\lambda}{\beta cos\theta} \quad (1)$$

Table 1. The crystallite size, strain, dislocation density, and lattice parameters of the pure and and Sb doped CuO.

Sample Name	D (nm)	Dislocation Density (x10^{-4})	Strain (x10^{-4})	Lattice parameters (Å)
S1	24.58	16.551	14.095	a=4,493 b=3,424 c=5,122
S2	17.86	31.350	19.400	a=4,485 b=3,406 c=5,115
S3	17.37	33.143	19.942	a=4,477 b=3,405 c=5.118

Where, λ is the wavelength of the X-rays (Cu Kα λ=1.5406 Å), k is the Scherrer constant taken as 0.9, β is the full width at half maximum (FWHM) and θ is the Bragg's diffraction angle [29]. It was observed that the crystallite size of the powders decreased with Sb doping and these values are 24.58 nm, 17.86 nm and 17.37 nm for the pure CuO, 1%, and 3% Sb doped CuO, respectively. While the crystallite size decreases with the doping of Sb in CuO, the dislocation density and strain gradually increases. The strain linearly increases due to the dopant atoms having a larger ionic radius than the host atom [12]. The lattice parameters of the monoclinic CuO and Sb doped CuO powders were calculated using monoclinic phase equation (Equation (2)) [25]:

$$\frac{1}{d^2} = \frac{1}{\sin^2\beta}\left(\frac{h^2}{a^2} + \frac{k^2\sin^2\beta}{b^2} + \frac{l^2}{c^2} - \frac{2hl\cos\beta}{ac}\right) \quad (2)$$

Small differences in lattice parameters were noted in samples with Sb doping. The lattice parameter variations (Table 1) may result from the difference in ionic radii of Cu^{2+} (0.73 Å) and Sb^{3+} (0.76 Å) ions (coordination number: VI) [30]. The lattice parameters of the pure and Sb doped CuO powders align with the values reported in its JCPDS card and literature [25, 31, 32].

3.2. Morphological properties

Surface morphology of the pure and Sb doped CuO powders synthesized by the CBD method were examined by FE-SEM and shown in the Figure 2. The pure CuO exhibits nano and micro-scale plate-like morphology with a thickness of approximately 100 nm.

These plates combine to form flower-like structures [6, 33-36]. Sb doping results in needle-like ends of the plate structures. Therefore, flower-like structures were formed by the combination of these needle-like plates. Futhermore, the SEM image clearly shows that the needle-like structures are more prominent in the 3% Sb-doped CuO sample. The thickness of the plates decreased with increasing Sb doping concentration. It was observed that Sb doping affected the morphological structure of the CuO. This alteration in surface morphology can significantly influence the physical and chemical properties of the material, including its catalytic and electronic behavior.

The elemental analysis of the powders was performed with EDX spectroscopy. The EDX spectra confirmed that the Sb successfully doped into the CuO structure (Figure 3).

3.3. Optical properties

Optical properties of the pure and Sb-doped CuO powders were determined by UV-Vis spectrophotometer in the range of 200 - 900 nm. The optical absorption spectra of the nano/micro powders are given in Figure 4. While the pure CuO and 1% Sb doped CuO have broad absorbance in the visible light region, a broad absorption peak is formed in the 3% Sb doped CuO sample between 215 and 600 nm wavelength. The improved absorption of the Sb-doped CuO sample may be attributed to the visible light-responsive nature of CuO [27].

Tauc method was used to determine the optical band gap energy (E_g) of the powders (Equation (3)) [15]:

$$(\alpha h\upsilon) = A(h\upsilon - E_g)^n \quad (3)$$

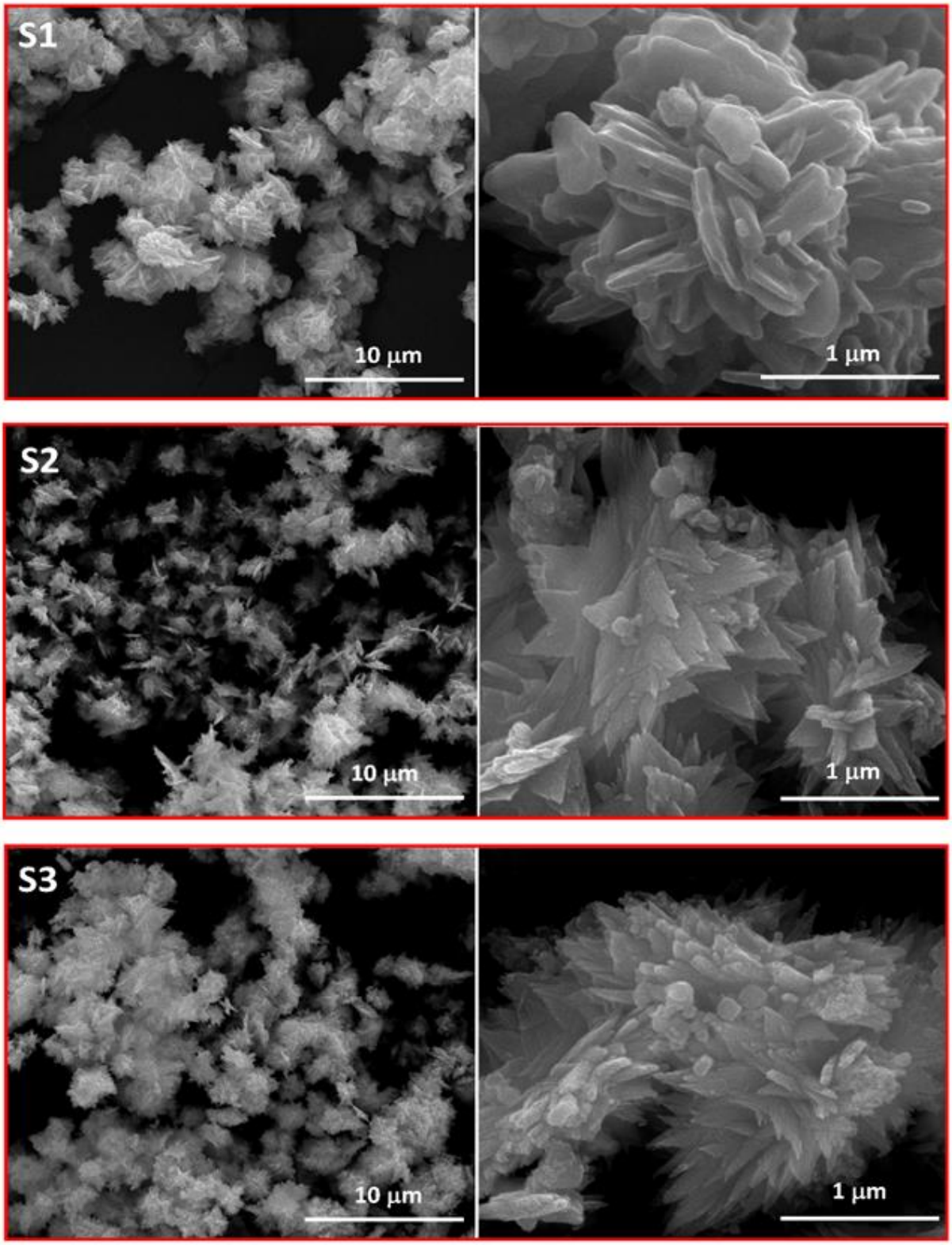

Figure 2. SEM images of the pure and Sb doped CuO powders and high magnification (on the right).

Where $h\nu$ is energy of a photon, α is the absorption coefficient, n determines the type of electronic transition [37], E_g is optical band gap energy, and A is a constant [15]. The optical band gap energy values were calculated as 1.58 eV, 1.66 eV and 1.95 eV for pure, 1%, and 3% Sb doped CuO powders, respectively (Figure 5). This means that the optical band gap energy of the CuO is found to increase with Sb doping. The increase in the E_g is known as blue shift [38, 39]. The variation in the optical band gap energy and the crystallite size depending on the Sb concentration is depicted in Figure 6. It has been observed that the crystal size changes inversely proportional to the band gap energy. The increase in band gap energy with decreasing particle size is attributed to the quantum confinement effect [40].

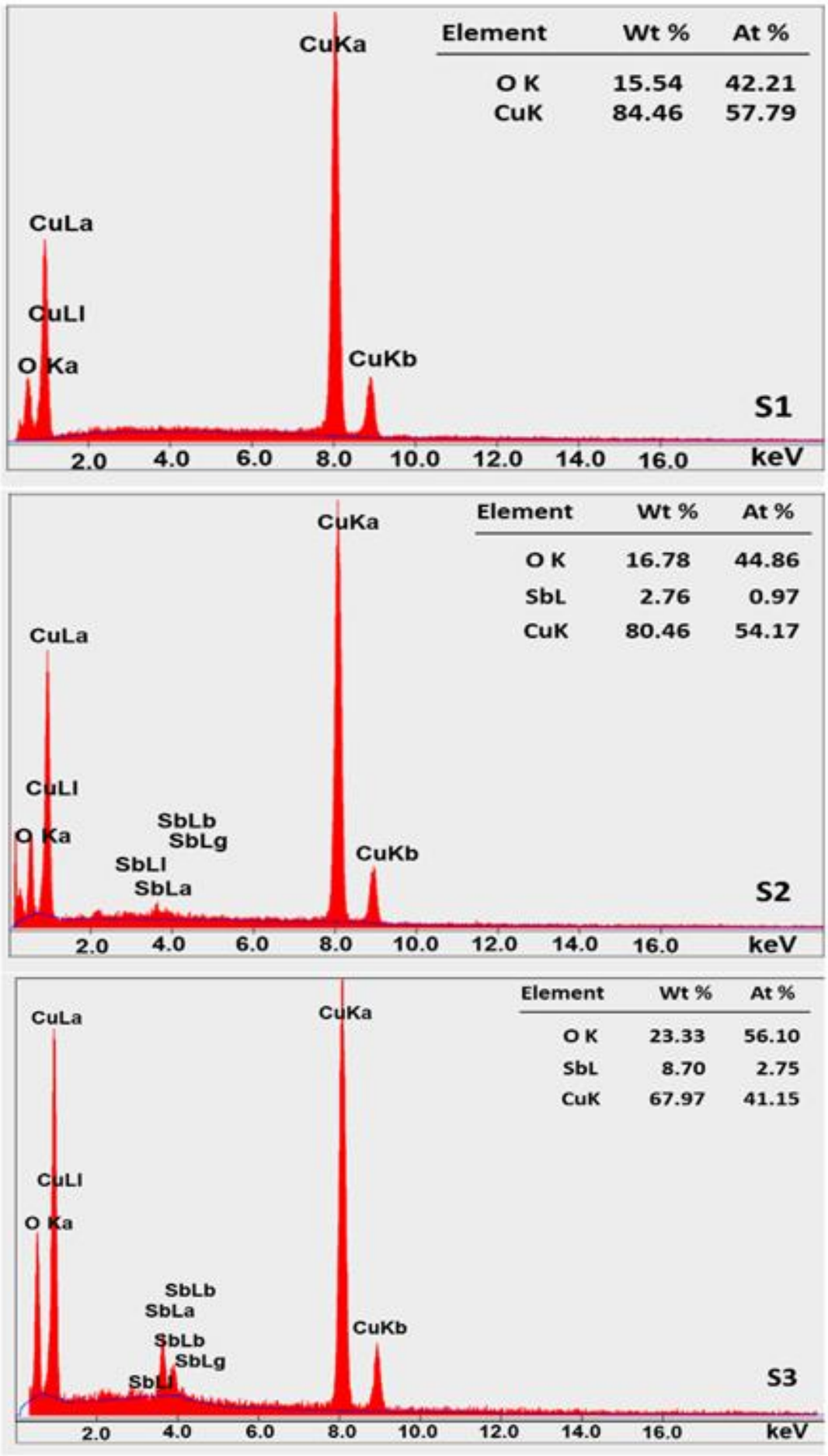

Figure 3. EDX spectra of the pure and Sb doped CuO powders.

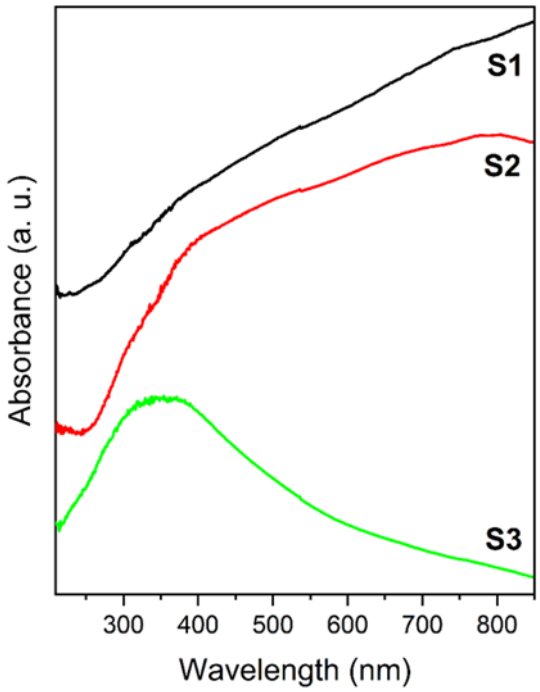

Figure 4. The optical absorbance spectra of the pure and Sb doped CuO powders.

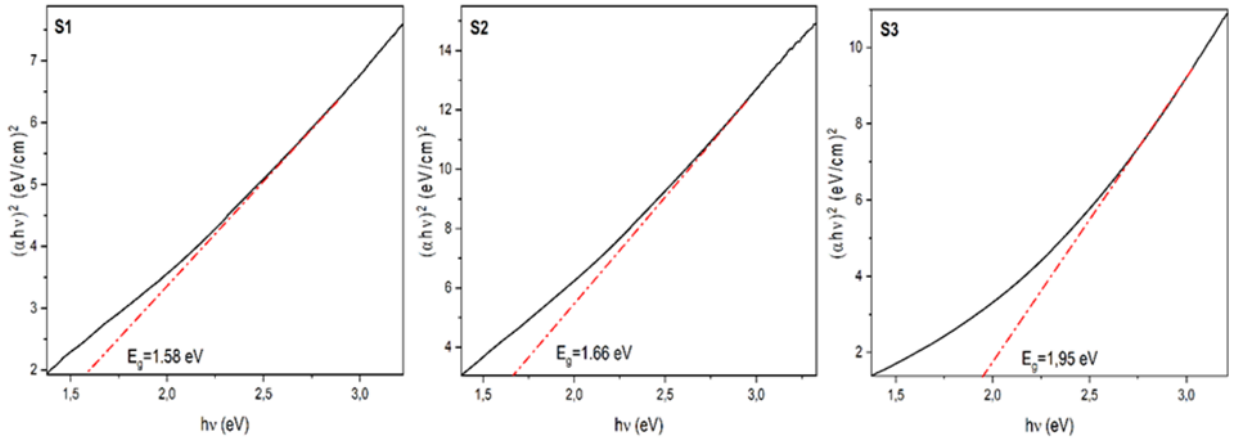

Figure 5. Tauc Plot of the pure and Sb doped CuO powders.

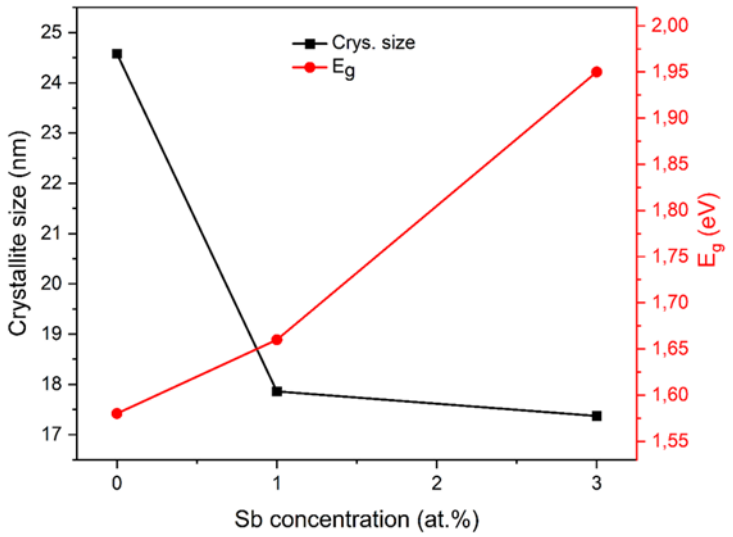

Figure 6. The variation in crystallite size and optical band gap energy depending on Sb concentration in CuO.

The extinction coefficient (k) and refractive index (n), linked to the electronic structure of a material, are crucial parameters for optoelectronic applications. The graph of extinction coefficient of the pure CuO and Sb doped CuO powders are shown in Figure 7. It was calculated by the following equation (Equation (4)) using the absorbance data of the powders [41]:

$$k = \frac{\alpha\lambda}{4\pi} \tag{4}$$

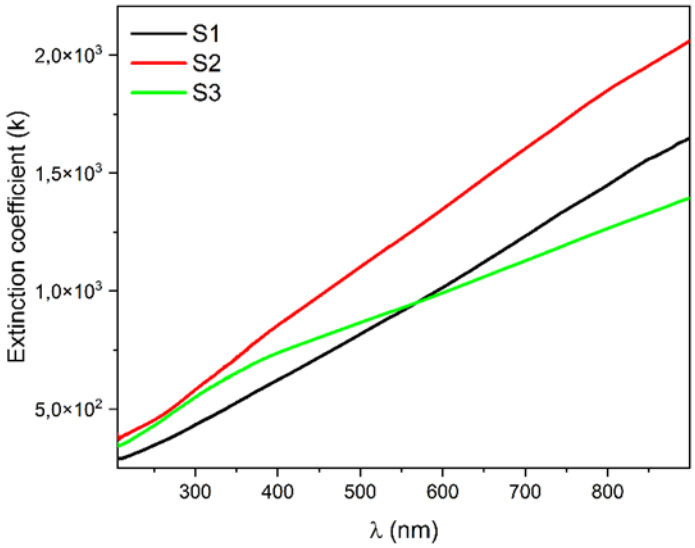

Figure 7. Variation of extinction coefficient of the pure and Sb doped CuO powders as a function of wavelength.

Where λ is wavelength of incident light and α is the absorption coefficient [41]. The extinction coefficient of all powders gradually increases with increasing of wavelength. An increase in the extinction coefficient indicates the existence of viable levels near conduction band [42]. The refractive index of the powders was calculated according to the following equation (Equation (5)) [43]:

$$n = 4.084 - 0.62E_g \tag{5}$$

The calculated refractive index values are 3.10, 3.05 and 2.88 for S1, S2 and S3 samples, respectively. The refractive index shows decreasing behavior with increasing Sb concentration.

The real and imaginary parts of the dielectric constant, which is related to the extinction coefficient and refractive index, were calculated using following equation (Equation (6)) and represented in Figure 8 [44, 45]:

$$\varepsilon_r = n^2 - k^2 \, , \varepsilon_i = 2nk \tag{6}$$

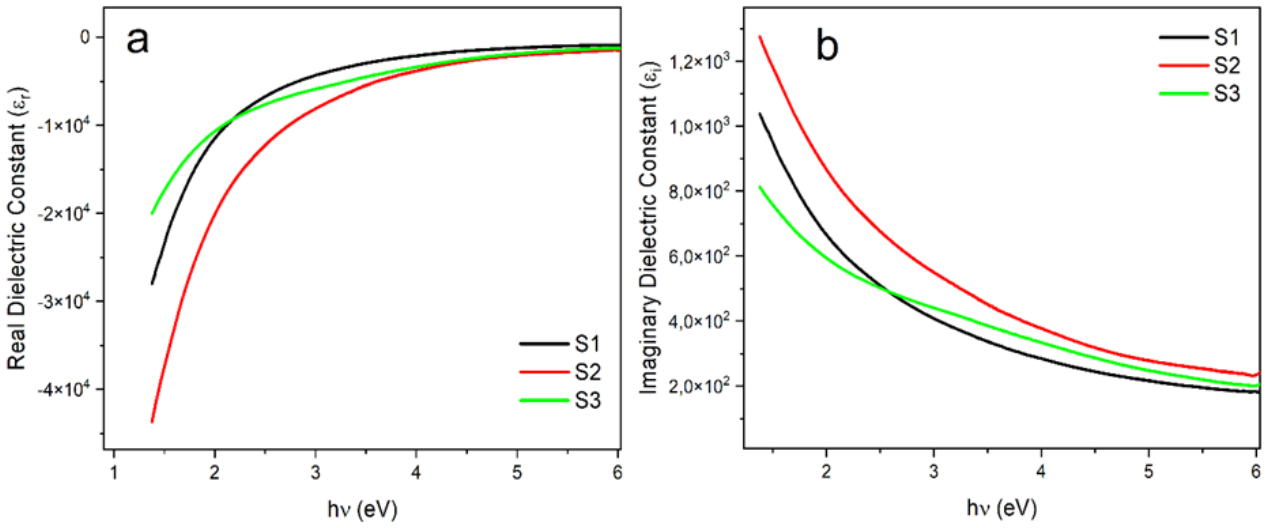

Figure 8. Variation of the real dielectric constant (a) and imaginary dielectric constant (b) as a function of photon energy.

The real part of the dielectric constant indicates the extent to which the material slows down the speed of light. The imaginary part of the dielectric constant indicates a dielectric material's energy absorption from an electric field via dipole motion [44]. It is clearly observed from Figure 8 (b) that the 1% Sb doped CuO absorbs light better than other samples and the imaginary part of the dielectric constant of all samples decreases upon photon energy increases.

4. Conclusion

The pure and Sb (1 and 3 at.%) doped CuO powders were synthesized using the CBD method. The synthesized powders are annealed at 450°C. The XRD analysis showed that both pure and Sb-doped CuO samples exhibited a monoclinic structure, with a decrease in crystallite size observed in the doped samples. The 3% Sb doped CuO with the smallest crystallite size shows the highest dislocation density and strain. The SEM analysis clearly showed that both pure and Sb doped CuO nano/micro powders exhibited a flower-like morphology. The thickness of the plates decreased with the effect of Sb doping. Ultimately, Sb doping influenced the morphology of CuO. The optical studies revealed that the value of band gap energy increases with Sb doping concentration. The E_g of the powders was calculated as 1.58 eV, 1.66 eV and 1.95 eV for pure, 1% and 3% Sb doped CuO samples, respectively. It was observed that the refractive index of the powders decreased as Sb doping increased. The pure and Sb doped CuO powders have potential for optoelectronic applications. This study will serve as a guide for future research on these applications.

Acknowledgement

This study has been partially supported by Mersin University Advanced Technology Education, Research and Application Center and ODTU MERLAB, Mersin, Türkiye.

Funding

This research received no external funding.

Conflicts of interest

The authors declare no conflicts of interest.

References

1. Al-Ghamdi, A. A., Khedr, M. H., Ansari, M. S., Hasan, P. M. Z., Abdel-Wahab, M. S., & Farghali, A. A. (2016). RF sputtered CuO thin films: Structural, optical and photo-catalytic behavior. Physica E: Low-dimensional Systems and Nanostructures, 81, 83-90. https://doi.org/10.1016/j.physe.2016.03.004
2. Wang, C., Fu, X. Q., Xue, X. Y., Wang, Y. G., & Wang, T. H. (2007). Surface accumulation conduction controlled sensing characteristic of p-type CuO nanorods induced by oxygen adsorption. Nanotechnology, 18(14), 145506. https://doi.org/10.1088/0957-4484/18/14/145506
3. Siavash Moakhar, R., Hosseini-Hosseinabad, S. M., Masudy-Panah, S., Seza, A., Jalali, M., Fallah-Arani, H., ... & Saliba, M. (2021). Photoelectrochemical water-splitting using CuO-based electrodes for hydrogen production: a review. Advanced Materials, 33(33), 2007285. https://doi.org/10.1002/adma.202007285
4. Wisz, G., Sawicka-Chudy, P., Sibiński, M., Starowicz, Z., Płoch, D., Góral, A., ... & Sosna-Głębska, A. (2021). Solar cells based on copper oxide and titanium dioxide prepared by reactive direct-current magnetron sputtering. Opto-Electronics Review, 29, 97-104. https://doi.org/10.24425/opelre.2021.139039
5. Jayatissa, A. H., Guo, K., & Jayasuriya, A. C. (2009). Fabrication of cuprous and cupric oxide thin films by heat treatment. Applied Surface Science, 255(23), 9474-9479. https://doi.org/10.1016/j.apsusc.2009.07.072
6. Quirino, M. R., Lucena, G. L., Medeiros, J. A., Santos, I. M. G. D., & Oliveira, M. J. C. D. (2018). CuO rapid synthesis with different morphologies by the microwave hydrothermal method. Materials Research, 21(6), e20180227. https://doi.org/10.1590/1980-5373-MR-2018-0227
7. Pramothkumar, A., Senthilkumar, N., Mercy Gnana Malar, K. C., Meena, M., & Vetha Potheher, I. (2019). A comparative analysis on the dye degradation efficiency of pure, Co, Ni and Mn-doped CuO nanoparticles. Journal of Materials Science: Materials in Electronics, 30(20), 19043-19059. https://doi.org/10.1007/s10854-019-02262-4
8. Jayaprakash, J., Srinivasan, N., Chandrasekaran, P., & Girija, E. K. (2015). Synthesis and characterization of cluster of grapes like pure and Zinc-doped CuO nanoparticles by sol–gel method. Spectrochimica Acta Part A: Molecular and Biomolecular Spectroscopy, 136, 1803-1806. https://doi.org/10.1016/j.saa.2014.10.087

9. Liao, Y., Wang, D., Wang, H., Wang, T., Zheng, Q., Yang, J., ... & Lin, D. (2019). Transformation of hardening to softening behaviors induced by Sb substitution in CuO-doped KNN-based piezoceramics. Ceramics International, 45(10), 13179-13186. https://doi.org/10.1016/j.ceramint.2019.03.254
10. Basith, N. M., Vijaya, J. J., Kennedy, L. J., & Bououdina, M. (2013). Structural, optical and room-temperature ferromagnetic properties of Fe-doped CuO nanostructures. Physica E: Low-dimensional Systems and Nanostructures, 53, 193-199. https://doi.org/10.1016/j.physe.2013.05.009
11. Yun, Y. D., Baek, S. K., Kim, J. S., Kim, Y. B., Jung, S. H., Kim, Y., & Cho, H. K. (2019). Optimal synthesis of antimony-doped cuprous oxides for photoelectrochemical applications. Thin Solid Films, 671, 120-126. https://doi.org/10.1016/j.tsf.2018.12.037
12. Ghosh, C. K., Popuri, S. R., Sarkar, D., & Chattopadhyay, K. K. (2011). Sb-doped CuAlO 2: widening of band gap and nonlinear J–E characteristics. Journal of Materials Science, 46, 1613-1621. https://doi.org/10.1007/s10853-010-4975-5
13. Baturay, Ş. (2020). Structural and optical properties of Sb doped CuO films. Academic Platform-Journal of Engineering and Science, 8(1), 84-90. https://doi.org/10.21541/apjes.605822
14. Sánchez-Rivera, M. J., Giner-Sanz, J. J., Pérez-Herranz, V., & Mestre, S. (2019). CuO improved (Sn, Sb) O_2 ceramic anodes for electrochemical advanced oxidation processes. International Journal of Applied Ceramic Technology, 16(3), 1274-1285. https://doi.org/10.1111/ijac.13149
15. Pandey, A., Yadav, P., Fahad, A., Kumar, P., & Singh, M. K. (2024). Sb dopant-induced modifications in CuO–ZnO nanocomposites: Optical, electrical and magneto-dielectric insights for optoelectronic applications. Ceramics International, 50(12), 21417-21428. https://doi.org/10.1016/j.ceramint.2024.03.253
16. Wang, X. D., Xu, Y. F., Chen, B. X., Zhou, N., Chen, H. Y., Kuang, D. B., & Su, C. Y. (2016). 3D cathodes of cupric oxide nanosheets coated onto macroporous antimony-doped tin oxide for photoelectrochemical water splitting. ChemSusChem, 9(20), 3012-3018. https://doi.org/10.1002/cssc.201601140
17. Baek, S. K., Kim, J. S., Kim, Y. B., Yoon, J. H., Lee, H. B. R., & Cho, H. K. (2017). Dual role of Sb-incorporated buffer layers for high efficiency cuprous oxide photocathodic performance: Remarkably enhanced crystallinity and effective hole transport. ACS Sustainable Chemistry & Engineering, 5(9), 8213-8221. https://doi.org/10.1021/acssuschemeng.7b01889
18. Qin, H., Zhang, Z., Liu, X., Zhang, Y., & Hu, J. (2010). Room-temperature ferromagnetism in CuO sol–gel powders and films. Journal of Magnetism and Magnetic Materials, 322(14), 1994-1998. https://doi.org/10.1016/j.jmmm.2010.01.021
19. Kaur, M., Muthe, K. P., Despande, S. K., Choudhury, S., Singh, J. B., Verma, N., ... & Yakhmi, J. V. (2006). Growth and branching of CuO nanowires by thermal oxidation of copper. Journal of Crystal Growth, 289(2), 670-675. https://doi.org/10.1016/j.jcrysgro.2005.11.111
20. Shashanka, R., & Kumara Swamy, B. E. (2020). Simultaneous electro-generation and electro-deposition of copper oxide nanoparticles on glassy carbon electrode and its sensor application. SN Applied Sciences, 2, 1-10. https://doi.org/10.1007/s42452-020-2785-1
21. Shinde, S. K., Yadav, H. M., Ghodake, G. S., Kadam, A. A., Kumbhar, V. S., Yang, J., ... & Kim, D. Y. (2019). Using chemical bath deposition to create nanosheet-like CuO electrodes for supercapacitor applications. Colloids and Surfaces B: Biointerfaces, 181, 1004-1011. https://doi.org/10.1016/j.colsurfb.2019.05.079
22. Ebin, B., Gençer, Ö., & Gürmen, S. (2013). Simple preperation of CuO nanoparticles and submicron spheres via ultrasonic spray pyrolysis (USP). International Journal of Materials Research, 104(2), 199-206. https://doi.org/10.3139/146.110853
23. Mote, V. D., Lokhande, S. D., Kathwate, L. H., Awale, M. B., & Sudake, Y. (2023). Structural, optical and magnetic properties of Mn-doped CuO nanoparticles by coprecipitation method. Materials Science and Engineering: B, 289, 116254. https://doi.org/10.1016/j.mseb.2022.116254
24. Raship, N. A., Sahdan, M. Z., Adriyanto, F., Nurfazliana, M. F., & Bakri, A. S. (2017). Effect of annealing temperature on the properties of copper oxide films prepared by dip coating technique. In AIP Conference Proceedings, 1788(1), 030121. https://doi.org/10.1063/1.4968374
25. Yildirimcan, S. (2023). Effect of ageing on electrical properties of Fe-doped CuO thin films deposited by spin coating technique. Indian Journal of Physics, 97(6), 1707-1716. https://doi.org/10.1007/s12648-022-02511-z
26. Ethiraj, A. S., & Kang, D. J. (2012). Synthesis and characterization of CuO nanowires by a simple wet chemical method. Nanoscale Research Letters, 7, 1-5. https://doi.org/10.1186/1556-276X-7-70
27. Berede, H. T., Andoshe, D. M., Gultom, N. S., Kuo, D. H., Chen, X., Abdullah, H., ... & Zelekew, O. A. (2024). Photocatalytic activity of the biogenic mediated green synthesized CuO nanoparticles confined into MgAl LDH matrix. Scientific Reports, 14(1), 2314. https://doi.org/10.1038/s41598-024-52547-w
28. Jhansi, K., Chandralingam, S., Reddy, M. N., Suvarna, P., Ashok, C., & Rao, M. K. (2016). CuO nanoparticles synthesis and characterization for humidity sensor application. Journal of Nanotechnology and Materials Science, 3(1), 10-14. https://doi.org/10.15436/2377-1372.16.020
29. Mustapha, S., Ndamitso, M. M., Abdulkareem, A. S., Tijani, J. O., Shuaib, D. T., Mohammed, A. K., & Sumaila, A. (2019). Comparative study of crystallite size using Williamson-Hall and Debye-Scherrer plots for ZnO nanoparticles. Advances in Natural Sciences: Nanoscience and Nanotechnology, 10(4), 045013.

https://doi.org/10.1088/2043-6254/ab52f7
30. Shannon, R. D. (1976). Revised effective ionic radii and systematic studies of interatomic distances in halides and chalcogenides. Foundations of Crystallography, 32(5), 751-767. https://doi.org/10.1107/S0567739476001551
31. Chethana, D. M., Thanuja, T. C., Mahesh, H. M., Kiruba, M. S., Jose, A. S., Barshilia, H. C., & Manjanna, J. (2021). Synthesis, structural, magnetic and NO_2 gas sensing property of CuO nanoparticles. Ceramics International, 47(7), 10381-10387. https://doi.org/10.1016/j.ceramint.2020.06.129
32. Siddiqui, H., Parra, M. R., & Haque, F. Z. (2018). Optimization of process parameters and its effect on structure and morphology of CuO nanoparticle synthesized via the sol− gel technique. Journal of Sol-Gel Science and Technology, 87, 125-135. https://doi.org/10.1007/s10971-018-4663-5
33. Buledi, J. A., Pato, A. H., Kanhar, A. H., Solangi, A. R., Batool, M., Ameen, S., & Palabiyik, I. M. (2021). Heterogeneous kinetics of CuO nanoflakes in simultaneous decolorization of Eosin Y and Rhodamine B in aqueous media. Applied Nanoscience, 11, 1241-1256. https://doi.org/10.1007/s13204-021-01685-y
34. Rani, M., Iqbal, J., Israr, M., Asim, M., Javaria, & Athar, T. (2022). CuO-decorated ZnO nanosheets with enhanced dielectric characteristics and visible light-driven photocatalytic activity towards organic pollutants. Journal of Nanoparticle Research, 24(10), 190. https://doi.org/10.1007/s11051-022-05559-4
35. Tamuly, C., Saikia, I., Hazarika, M., & Das, M. R. (2014). Reduction of aromatic nitro compounds catalyzed by biogenic CuO nanoparticles. RSC Advances, 4(95), 53229-53236. https://doi.org/10.1039/c4ra10397a
36. Çetinkaya, S., Erat, S., & Aycibin, M. (2023). Simple and low-cost solution method for cobalt doped CuO nanostructured powder. Advanced Engineering Science, 3, 188-195.
37. Sangiorgi, N., Aversa, L., Tatti, R., Verucchi, R., & Sanson, A. (2017). Spectrophotometric method for optical band gap and electronic transitions determination of semiconductor materials. Optical Materials, 64, 18-25. https://doi.org/10.1016/j.optmat.2016.11.014
38. Babu, M. H., Podder, J., Dev, B. C., & Sharmin, M. (2020). p to n-type transition with wide blue shift optical band gap of spray synthesized Cd doped CuO thin films for optoelectronic device applications. Surfaces and interfaces, 19, 100459. https://doi.org/10.1016/j.surfin.2020.100459
39. Rehman, S., Mumtaz, A., & Hasanain, S. K. (2011). Size effects on the magnetic and optical properties of CuO nanoparticles. Journal of Nanoparticle Research, 13, 2497-2507. https://doi.org/10.1007/s11051-010-0143-8
40. Koshy, J., & George, K. C. (2015). Annealing effects on crystallite size and band gap of CuO nanoparticles. International Journal of NanoScience and Nanotechnology, 6(1), 1-8.
41. Mayakannan, M., Gopinath, S., & Vetrivel, S. (2020). Synthesis and characterization of antibacterial activities nickel doped cobalt oxide nano particles. Materials Chemistry and Physics, 242, 122282. https://doi.org/10.1016/j.matchemphys.2019.122282
42. Dwech, M. H., Aadim, K. A., & Mohsen, M. T. (2019, August). The effect of a number of laser pulses on optical properties of CuO thin films deposited by pulsed laser deposited (PLD) technique at 673K. AIP Conference Proceedings, 2144(1), 030024. https://doi.org/10.1063/1.5123094
43. Ravindra, N. M., Auluck, S., & Srivastava, V. K. (1979). On the Penn gap in semiconductors. Physica status solidi (b), 93(2), K155-K160. https://doi.org/10.1002/pssb.2220930257
44. Bharti, D. B., & Bharati, A. V. (2017). Synthesis of ZnO nanoparticles using a hydrothermal method and a study its optical activity. Luminescence, 32(3), 317-320. https://doi.org/10.1002/bio.3180
45. Rami, J. M., & Patel, C. D. (2023) Exploration of significant optical parameters of selected metal oxide nanoparticles using optical spectroscopy. Nano World Journal, 9, 601-605. https://doi.org/10.17756/nwj.2023-s1-116